AIAA JOURNAL
Vol. 49, No. 2, February 2011

Fluid–Structure Interaction Model for Low-Frequency Synthetic Jets

Charles E. Seeley,* Yogen Utturkar,* Mehmet Arik,* and Tunc Icoz*
GE Global Research, Niskayuna, New York 12309

DOI: 10.2514/1.J050433

Advancements in microelectronics have increased circuit board heat densities to the point where active cooling is required. Synthetic jets offer interesting capabilities for localized active cooling of electronics due to their compact size, low cost, and substantial cooling effectiveness. The design of synthetic jets for specific applications requires practical design tools that capture the strong fluid–structure interaction without computationally long run times. There is particular interest in synthetic jets that have a low operating frequency to reduce noise levels. This paper describes how common finite elements and codes can be used to calculate parameters for a synthetic jet fluid–structure interaction model that only requires a limited number of degrees of freedom and is solved using a direct approach for low-frequency synthetic jets. Extensive tests are performed with the synthetic jet in vacuum to measure deflection, in ambient air to measure pressure and exit velocity, and impinging on a heated surface to measure heat transfer enhancement. The test results are compared with the fluid–structure interaction model results for validation, and agreement is found to be good in the frequency range of interest from 200 to 500 Hz.

Nomenclature

A	=	area, m^2
c	=	damping coefficient, N/(m/s)
D	=	synthetic jet diameter, m
d	=	piezoelectric charge coefficient, m/m per V/m
$\bar{E}$	=	electric field, V/m
$\mathbf{F}$	=	force vector, N
f	=	force coefficient, N
i	=	current, A
$\mathbf{K}$	=	stiffness matrix, N/m
k	=	stiffness coefficient, N/m
$\mathbf{M}$	=	mass matrix, kg
m	=	mass coefficient, kg
P	=	absolute pressure, Pa
p	=	gauge pressure or power, Pa or W
Q	=	heat transfer rate, W
R	=	specific gas constant, J/(kg · K)
Re	=	Reynolds number
T	=	temperature, K
t	=	time or thickness, s or min.
u	=	displacement, m
$\mathbf{u}$	=	displacement vector, m
V	=	volume, m^3
v	=	voltage, V
W	=	synthetic jet width, m
x, y, z	=	coordinates, m
α	=	coefficient of thermal expansion, m/m per °C
β	=	influence coefficient, N/Pa or N/V
ζ	=	damping ratio
μ	=	dynamic viscosity, Pa · s
ρ	=	density, kg/m^3
σ	=	stress, Pa
ϕ	=	mode shape
ω	=	natural frequency, rad/s

Received 11 February 2010; revision received 8 July 2010; accepted for publication 25 August 2010.

*Energy and Propulsion Technologies.

I. Introduction

SYNTHETIC jets are zero net mass flow devices that synthesize unsteady jet flow from an ambient fluid. They are useful for flow control [1], triggering turbulence in boundary layers [2], and heat transfer applications [3–5]. In the case of heat transfer applications, the cooling process is facilitated by direct impingement of vortex dipoles, created by the synthetic jet, on heated surfaces [6] or by employing the synthetic jet to enhance the performance of existing cooling circuits [7]. The application of synthetic jets for the active cooling of microelectronics is particularly compelling due to trends toward higher heat densities as a result of increased functionality in smaller packages. Although various actuators for synthetic jets have been evaluated [5], piezoelectric bimorph actuators are attractive for electronics cooling due to their low cost and simplicity.

A typical synthetic jet configuration is shown in Fig. 1 that has two piezobimorph actuators with a cavity of air in between. The disks are energized to reduce or expand the cavity volume at a low driving frequency in the 200 to 500 Hz range to ingest and expel the surrounding air through an orifice. This frequency range is of particular interest due to the reduced human sensitivity to noise, resulting in good heat transfer performance at lower perceived noise levels. The resulting pulsating jet of air has positive momentum due to the asymmetry of the flow in and out of the orifice. The jet is directed to impinge on a surface, such as a printed circuit board assembly, to enhance the heat transfer. Although the synthetic jets are small in size, they create significantly enhanced heat transfer in comparison with natural- or low-speed forced convection cooling [7]. They do not require an external fluid source, and they have no sliding or rotating parts.

Development of a comprehensive mathematical model to predict the performance characteristics of a synthetic jet is challenging due to the strong interactions between the electromechanical coupling in the piezoelectric actuator, the dynamic response of the flexible bimorph disk, the pressure of the air in the chamber that resists the motion of the disk, the velocity of the jet of air through the orifice, and the resulting impingement heat transfer enhancement. A monolithic approach to solve the fluid–structure interaction (FSI) problem, where the governing equations result from fine discretization of the fluid and structural domains, is not practical due to the solver code complexity and development effort required. A partitioned approach, where the equations governing the flow and displacement of the structure are solved separately [such as with independent finite element analysis (FEA) and computational fluid dynamics (CFD) codes] and iterations are made to obtain convergence at the fluid–structure boundaries, is also not practical for design studies due to the model sizes and computationally long run times. The flow dynamics

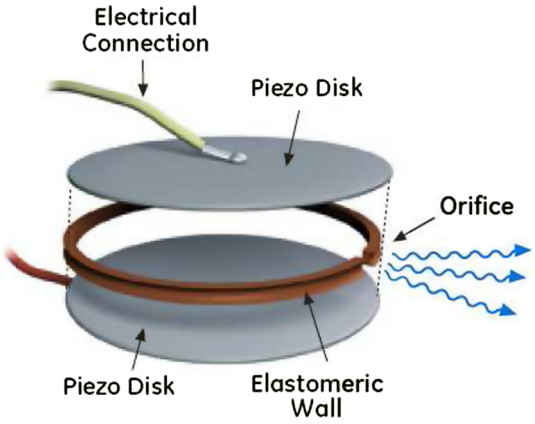

Fig. 1 The synthetic jet has a pair of piezoelectric disks that deform to change the volume of the cavity of air between them and force air in and out of the orifice.

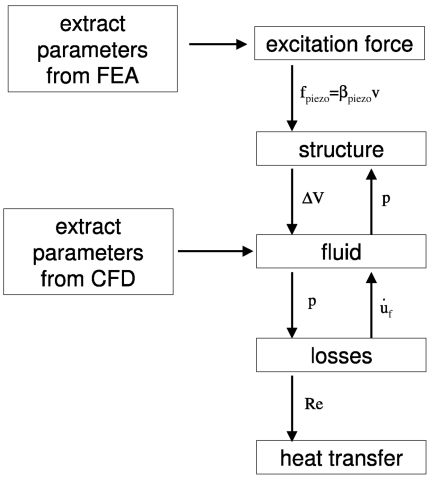

Fig. 2 Block diagram of the interaction between the different disciplines in the FSI model.

of synthetic jets have been investigated in detail by a number of authors [1,2,4,8–13]. These efforts investigated important features of the flowfield, including vortex formation, velocity profiles, and pressure losses. However, they have not attempted to couple all of the domains that govern synthetic jet performance, including piezoelectric, structural, fluid, and heat transfer. Previous efforts by the authors have included only one-way coupling from the structure to either an acoustic fluid [14] or a prescribed moving CFD mesh [15]. Gallas et al. [16] developed a lumped parameter model based on an equivalent circuit that included aspects of both the fluid and the structure. Clingman [17] used another approach based on fundamental thermodynamic relationships. Sharma [18] also developed an analytical model with multidisciplinary coupling.

The model developed in this paper is an effort to capture the coupling between the piezoelectric, structural, fluids, and heat transfer domains for synthetic jets, operating well below the Helmholtz frequency, that is appropriate for use as a practical design tool with short computational run times. At the same time, the model attempts to be accurate and leverage the use of commercial finite element (FE) and CFD codes without the computationally long run times. This is accomplished by extracting critical structural parameters, such as stiffness and natural frequency, from a detailed FE model and extracting orifice loss parameters from a detailed CFD model. These parameters are then used as coefficients for a set of equations solved simultaneously to calculate the fully coupled transient response of the synthetic jet in a monolithic approach with a limited number of degrees of freedom. The piezoelectric, structural, and fluid domains are based strictly on theory, with no tuning parameters. The heat transfer aspect is based on an empirical correlation using lab data. Following is a description of the model development, validation tests that were performed, and a comparison of the model and test results.

II. Synthetic Jet Fluid–Structure Interaction Model

The goal of the FSI model is to develop a practical design tool to explore the synthetic jet design space and give useful trends, with quick turnaround, to improve synthetic jet performance with reasonable accuracy in the frequency range of interest. It is also of interest to leverage commercial FEA and CFD software tools where possible. A block diagram of the approach is found in Fig. 2. FE and CFD codes are used independently to provide parameters for the limited degree-of-freedom equations that govern each domain. The domains are then coupled by solving the governing equations simultaneously, using a direct approach to predict the performance of the synthetic jet. Details of the approach and the development of the relevant equations of motion are outlined next.

A. Structural Model Development

The structural equations of motion, based on a FE approach, are given as

$$\mathbf{M}\,\ddot{\mathbf{u}}_s + \mathbf{K}\mathbf{u}_s = \mathbf{F}_{\text{piezo}} + \mathbf{F}_{\text{press}} \tag{1}$$

where $\mathbf{M}$ and $\mathbf{K}$ are the mass and stiffness matrices, $\mathbf{u}_s$ is the vector of nodal displacements of the structure (subscript s), and $\mathbf{F}_{\text{piezo}}$ and $\mathbf{F}_{\text{press}}$ are the forces due to the piezoelectric actuation and internal pressure, respectively. The in-plane stress generated by energizing the piezoelectric layer with an electric field through the thickness σ_{piezo} is calculated in the FE code using a thermal stress analogy for convenience:

$$\sigma_{\text{piezo}} = \alpha\Delta T = \frac{d_{31}}{t_{\text{piezo}}}v(t) \tag{2}$$

where α is the coefficient of thermal expansion that represents the piezoelectric coupling coefficient d_{31}, and the temperature change ΔT represents the time varying voltage $v(t)$. The quantity t_{piezo} is the thickness of the piezoelectric layer. Natural frequencies ω_i and their corresponding mode shapes ϕ_i are found by solving the associated eigenvalue problem:

$$(\mathbf{K} - \omega_i^2\mathbf{M})\phi_i = 0 \tag{3}$$

The FE code is used to perform a modal analysis to determine the natural frequency of the structure ω, corresponding to the mode shape of interest in the frequency range desired. Next, a physical point on the structure is selected to represent the displacement u_s as a master degree of freedom for that mode shape, such as the center of the piezoelectric disk. A unit nodal force $\bar{f}$ is applied to this point, yielding a displacement $\bar{u}_k$ that is calculated from a static analysis using the FE code. Assuming the static mode shape is representative of the dynamic mode shape excited in the frequency range of interest, a representative stiffness k is calculated from

$$k = \frac{\bar{f}}{\bar{u}_k} \tag{4}$$

Then, using the well-known Rayleigh quotient [19], a representative mass m is found, since k and ω are now known:

$$\omega^2 = \tfrac{k}{m} \tag{5}$$

Next, the unit force is removed and a unit voltage $\bar{v}$ is applied to the piezoelectric material in the FE model as a separate static analysis. The resulting displacement is recorded as $\bar{u}_{\text{piezo}}$, which is used to calculate the piezoelectric influence coefficient β_{piezo}:

$$\beta_{\text{piezo}} = k\bar{u}_{\text{piezo}} \tag{6}$$

where the representative force due to the piezoelectric actuation f_{piezo} is now found from

$$f_{\text{piezo}} = \beta_{\text{piezo}} v \tag{7}$$

where v is the applied voltage. In another load case, the unit voltage is removed and a uniform unit pressure $\bar{p}$ is applied to the structure in a manner that represents the internal pressure of the synthetic jet. The resulting displacement is recorded as $\bar{u}_{\text{press}}$, which is used to calculate the pressure influence coefficient β_{press}:

$$\beta_{\text{press}} = k\bar{u}_{\text{press}} \tag{8}$$

where the representative force due to the pressure actuation f_{press} is found from

$$f_{\text{press}} = \beta_{\text{press}} p \tag{9}$$

Note that p in this context represents the differential (or gauge) pressure inside the synthetic jet cavity. The absolute pressure P is the sum of the differential pressure p and the ambient atmospheric pressure P_0:

$$P = P_0 + p \tag{10}$$

Using the parameters found from the FEA, the single-degree-of-freedom structural equation of motion, based on summation of the forces according to Newton's second law, is now given as

$$m\ddot{u}_s + c\dot{u}_s + ku_s = \beta_{\text{piezo}} v + \beta_{\text{press}} p \tag{11}$$

where all of the parameters, m, k, β_{piezo}, and β_{press}, are determined from the proceeding load cases from the standard application of a commercial FE code. The quantity c, which represents the structural damping, is the only unknown structural parameter that is determined from

$$c = 2m\omega\zeta \tag{12}$$

where m and ω are already known and ζ is the damping ratio due to structural damping. It is the result of molecular motion, friction, viscoelastic material behavior, and other complex mechanisms that are not practical to model in this context, so ζ is determined empirically from test data.

A FE model of the synthetic jet with no fluid effects was built using the ANSYS [20] FE software package to obtain the structural parameters needed later for the FSI model. The FE model was a one-eighth symmetric model, as illustrated in Fig. 3. It comprised approximately 6500 brick elements. It was assumed that the orifice had no effect on the structural parameters in the absence of air, so it was not included in the model.

B. Ideal Gas Model

Energizing the piezoelectric material in the frequency range of interest causes a periodic deflection of the flexible structure that surrounds the chamber of air, which results in a net change in volume and forces air in and out of the orifice. The total volume of the chamber is the initial, undeformed volume V_0 plus the change in volume due to the deflection of the structure ΔV:

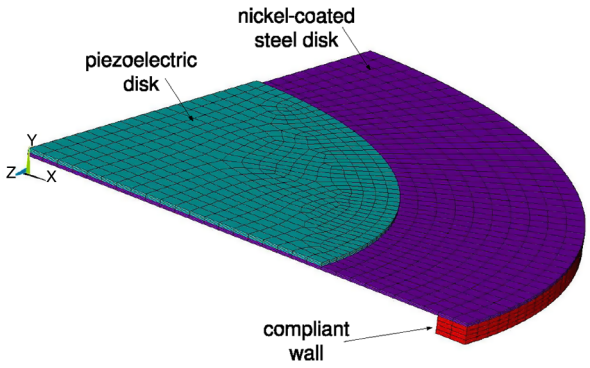

Fig. 3 FE model of synthetic jet using one-eighth symmetry.

$$V = V_0 + \Delta V \tag{13}$$

The change in volume is calculated based on the effective area of the structure A_{eff} and the deflection:

$$\Delta V = A_{\text{eff}} u_s \tag{14}$$

where A_{eff} is calculated based on the volume created by deformation of the structure in its dynamic mode shape ϕ in the frequency range of interest. It is found from

$$A_{\text{eff}} = \frac{\int_A \phi \, \mathrm{d}A}{\bar{u}} \tag{15}$$

where A is the surface area of the structure, ϕ is the mode shape, and $\bar{u}$ is its corresponding unit deflection. Assuming that the working fluid is air, or some other ideal gas, the pressure P is related to the volume V and temperature T through the ideal gas law:

$$PV = m_F RT \tag{16}$$

where m_F is the mass of the fluid and R is the specific gas constant. The Mach number at the highest expected exit velocity in the frequency range of interest is less than 0.1, so the air is assumed to be incompressible. This indicates that the density ρ is constant, so the mass of the fluid in the chamber m_F is found as

$$m_F = \rho V \tag{17}$$

The pressure in the chamber is created due to the rapid change in volume created by energizing the piezoelectric disks, so the differential form of the idea gas law, with respect to time, is more useful:

$$\frac{\mathrm{d}P}{\mathrm{d}t} V + P \frac{\mathrm{d}V}{\mathrm{d}t} = \frac{\mathrm{d}m_f}{\mathrm{d}t} RT + m_f R \frac{\mathrm{d}T}{\mathrm{d}t} \tag{18}$$

Here, it is assumed that the change in temperature with each cycle of the synthetic jet is negligible, so the change in temperature with respect to time is assumed to be zero, $\frac{\mathrm{d}T}{\mathrm{d}t} = 0$. In addition to being consistent with empirical observations, this assumption also avoids issues with excessive temperature changes observed from calculations in other works that may not be physically realistic [17]. The change in volume with respect to time is

$$\frac{\mathrm{d}V}{\mathrm{d}t} = A_{\text{eff}} \dot{u}_s \tag{19}$$

The change in mass with respect to time of the control volume within the chamber is due to the mass of air that exits and reenters the chamber through the orifice at each ingestion/expulsion cycle:

$$\frac{\mathrm{d}m_f}{\mathrm{d}t} = \rho A_{\text{orifice}} \dot{u}_f \tag{20}$$

where the quantity u_f is the position of a representative particle of the fluid at the orifice, and the dot notation is differentiation with respect to time, so $\dot{u}_f$ is the velocity of the fluid at the orifice. It is assumed that the velocity profile across the orifice is uniform. The quantity A_{orifice} is the cross-sectional area of the orifice.

C. Loss Model Development

Next, a practical loss model is developed to relate the differential pressure p to the orifice exit velocity $\dot{u}_f$. Note that the overdot notation, indicating differentiation with respect to time, is used to be consistent with the structural model. To start with, consider a differential fluid element that surrounds the orifice, illustrated in Fig. 4, with pressure P, net shear and normal stress τ, and dimensions Δx, Δy, and Δz. Assuming that body forces, such as gravitation and electrical and magnetic forces, are negligible and that the flow is one-dimensional along the x axis through the orifice; the forces on the fluid are summed using Newton's second law, yielding a form of the well-known Navier–Stokes momentum equation [21]:

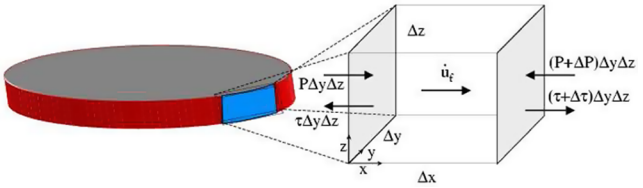

Fig. 4 Fluid element used to derive loss model for FSI model.

$$-\frac{\Delta P}{\Delta x}+\mu\frac{\Delta \dot{u}_f}{\Delta y^2}=\rho\frac{\Delta \dot{u}_f}{\Delta t}+\rho\frac{\Delta \dot{u}_f}{\Delta x}\dot{u}_f \tag{21}$$

where the velocity $\dot{u}_f$ is assumed to be uniform across the orifice, ρ is the density, and μ is the dynamic viscosity coefficient. Introducing the scaling parameters D and W for Δx and Δy, respectively, into the momentum equation and solving for the pressure drop yields

$$\Delta P=\underbrace{-D\rho\Delta\ddot{u}_f}_{\text{unsteady}}-\underbrace{\rho\Delta\dot{u}_f^2}_{\text{dynamic pressure}}+\underbrace{\frac{D}{W^2}\mu\Delta\dot{u}_f}_{\text{viscous}} \tag{22}$$

The first term on the right-hand side of Eq. (22) is the unsteady term due to the change in velocity of the air with respect to time. Although the condition of steady flow through an orifice is well known, the condition of unsteady flow through an orifice is not nearly as well understood. Furthermore, the term is vital to the analysis of synthetic jets, since the unsteady term tends to dominate the other terms that contribute to the pressure drop, especially at higher frequency due to the oscillating flow. The second term is due to the dynamic pressure from the motion of the air and is related to the kinetic energy of the flow. Continuity must be maintained through the orifice, even as streamlines bend and separate past the orifice. Therefore, a non-dimensional scaling factor is identified for the dynamic pressure term that relates to the continuity of flow through the orifice and the scaling of losses incurred due to the convergence of the streamlines near the orifice, known as the vena contracta effect. The pressure drop through the orifice is now

$$\Delta P=-D\rho\ddot{u}_f-\rho\left[\left(\frac{D}{W}\right)^2-1\right]\dot{u}_f^2\text{sign}(\dot{u}_f)+\frac{D}{W^2}\mu\dot{u}_f \tag{23}$$

where the sign( ) function accounts for flow in both directions for the dynamic pressure. The third term is the viscous term. Since the previous expression assumes W as the length scale along the y axis, it is restricted to a two-dimensional slice of the flowfield. To generalize the result to a three-dimensional (3-D) flowfield through the orifice, the hydraulic diameter D_H is used to replace the orifice width W in the third term:

$$p=-D\rho\Delta\ddot{u}_f-\rho\left[\left(\frac{D}{W}\right)^2-1\right]\Delta\dot{u}_f^2\text{sign}(\dot{u}_f)+\frac{D}{D_H^2}\mu\Delta\dot{u}_f \tag{24}$$

where p is the pressure drop ΔP, from Eq. (11). Note that the viscous term neglects the impact of the driving frequency on the wall shear stress coefficient μ. Although this assumption might not hold true over a wide range of frequencies, it is accurate over the narrow range of frequencies considered for this study, as will be illustrated shortly (especially below 500 Hz). The previous expression is the loss model of the unsteady flow through the orifice of a synthetic jet that relates the pressure inside the synthetic jet chamber to the velocity and acceleration of the flow. It is further specialized by introducing three coefficients, C_1, C_2, and C_3, that facilitate fitting the loss model with geometric scaling factors to a sophisticated 3-D CFD model of a synthetic jet:

$$P=-C_1D\rho\ddot{u}_f-C_2\rho\left[\left(\frac{D}{W}\right)^2-1\right]\dot{u}_f^2\text{sign}(\dot{u}_f)+C_3\frac{D}{D_H^2}\mu\dot{u}_f \tag{25}$$

A matrix of 3-D CFD analyses was run over a range of frequencies from 200 to 1000 Hz and 20 to 60 V to provide data to fit the coefficients C_1, C_2, and C_3 for the previous equations. The CFD model simulated the time-dependent flow from a synthetic jet impinging on a flat, 1 in.^{2} plate using the Icepak 4.4.8 [22] CFD software package, which was employed for the computations. Figure 5 illustrates the computational domain, which comprised hollow blocks representing the disk actuators, an elastomeric wall, and a fluid block representing the orifice. The flow across the jet orifice was resolved by 40 grid points along the width (8 mm) and 15 grid points along the height (1 mm) of the jet. The Reynolds number Re, based on the maximum expected time-averaged exit velocity and the orifice hydraulic diameter, fell within the laminar regime for internal flow ($Re < 2000$) [23]. Each actuation cycle was resolved with 20 time steps. The movement of the disks during actual jet operation was translated into a time-varying velocity boundary condition based on the mode shape of the disk that incorporated the simply supported boundary conditions around the edge and at a peak in the middle, and a sinusoidal excitation in time. This velocity condition was imposed on the CFD model on the surface of the jet disks facing the jet chamber (marked in Fig. 5).

The pressure inside the jet was dictated by the following factors: 1) skin friction occurring on the chamber/orifice walls, 2) spatial change in fluid momentum due to convergence/divergence occurring around the orifice (due to the nonlinear term), and 3) acceleration/deceleration due to the unsteadiness in the flowfield. While skin friction was inherent to all internal flows, causes 2 and 3 were attributed to the geometrical shape of the jet and its frequency-driven input, respectively.

D. Heat Transfer

The cooling performance of the synthetic jet that is directed toward an electric film heater is defined as an enhancement factor (EF), which is the ratio of heater power with the synthetic jet energized Q_{sj} to heater power with only natural convection cooling Q_{nc} at constant temperature. In other words, EF represents how much more power can be dissipated by the heater with the synthetic jet cooling while maintaining the same temperature compared with natural convection:

$$\text{EF}=\frac{Q_{\text{sj}}}{Q_{\text{nc}}} \tag{26}$$

Note that EF is defined only for the side of the heater that is impinged upon by the synthetic jet. Also, there are several heat transfer mechanisms at work here. The unsteady jet of air from the orifice impinges on the heater surface, disturbs the boundary layer, and increases the local heat transfer coefficient. Vortices that are shed due to the jet create a transport mechanism that carries away heat from the surface. Also, the motion of the air due to the synthetic jet generally enhances mixing and diffusion. Modeling the detailed physics of the flow dynamics to describe these heat transfer mechanisms is beyond the scope of this effort. Instead, an empirical

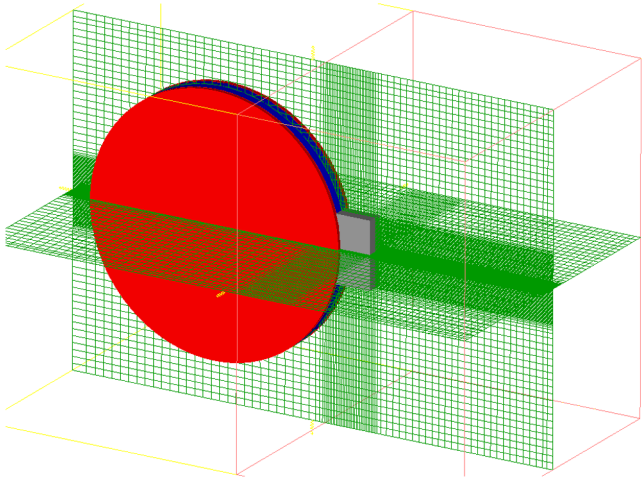

Fig. 5 CFD model for simulating time-dependent synthetic jet flowfield.

correlation is used based on a wealth of heat transfer test data available from testing many different devices. The correlation is defined as

$$\mathrm{EF} = C_0 Re^{C_1} \bar{u}^{C_2} \tag{27}$$

where Re is the Reynolds number, and $\bar{u}$ is the nondimensional deflection as a function of the deflection amplitude u, effective area A_{eff}, and the original volume V_0 ($\bar{u} = uA_{\text{eff}}/V_0$). It can also be considered the relative amplitude of the change in volume over each cycle at the operating condition of interest.

E. Fluid–Structure Interaction Implementation

In summary, there are three unknowns: the deflection of the structure u_s, the exit velocity of the fluid $\dot{u}_f$, and the pressure inside the cavity p. Three primary equations describe the operation of the synthetic jet: the structural equation (11), the ideal gas equation (18), and the loss equation (25). These equations are coupled through the forces due to piezoelectric actuation, the change in volume due to the motion of the structure, and pressure buildup in the cavity that forces air out through the orifice and feeds back onto the structure. This set of equations is a set of nonlinear, implicit differential equations, making them challenging to solve. The equations are nonlinear due to the products of P and V in the differential form of the ideal gas law and the dynamic pressure term in the loss model. They are also implicit, since the dependent variables u_s, u_f, P, and V cannot be isolated into a standard form [24]. The model was implemented in MATLAB [25] using the ode15i implicit differential equation solver with the Jacobian, calculated using a finite difference approach for the time domain solution. The initial conditions must be chosen carefully to prevent large transient behavior from disrupting the desired steady-state solution. The solution needed at least 10 cycles for the transient effects to die out, but the solver failed to converge after more than 10 cycles for unknown reasons. As a workaround, the solution was restarted several times after only three cycles, using the conditions at the end of the third cycle as a new guess for the initial conditions. After several restarts, the improved guess for the initial conditions minimized the transient effects, leading to a steady-state solution.

III. Model Validation

Once the FSI model was formulated and implemented in a MATLAB code, the next step was to check the predictive capability of the model against experimental data from lab tests to characterize the synthetic jet performance. Several tests were conducted, such as vacuum tests, pressure tests, and exit velocity and heat transfer tests. Further details of the tests are found in another paper [26]. In all cases, a synthetic jet with a pair of piezoelectric monomorph disks was used for validation. The diameter of the piezoelectric disk, was 20 mm with a thickness of 110 μm, and was mounted on nickel-coated steel disks with a diameter of 30 mm, with a thickness of 100 μm. The silicone was 1×1 mm around the circumference of the synthetic jet. In general, the experimental error was characterized as follows. The error was the difference between the measured value and its actual value:

$$\text{error} = \text{measured value} - \text{actual value} \tag{28}$$

and the relative experimental error was calculated as

$$\text{relative error} = \frac{\text{error}}{\text{actual value}} \tag{29}$$

Specific consideration of the relative experimental error for each validation test is elucidated in the sections that follow, which describe the validation tests and compare with the FSI model.

A. Validation in Vacuum

Energizing the synthetic jet in a vacuum allowed the frequency response to be determined of the structure alone without any fluid effects. The vacuum test setup comprised a vacuum chamber approximately 300 mm in diameter with a clear acrylic top. A vacuum pump was used to reduce the pressure inside the chamber to the desired level. The synthetic jet was placed in the vacuum chamber using feedthroughs for the electrical connections. A function generator created line level sine sweeps across the frequency range of interest with a gain to the required voltage for the synthetic jets supplied by an amplifier. The disk velocity at the center of one piezoelectric disk was measured using a laser vibrometer that was positioned outside the chamber but had line of sight to the synthetic jet through the clear acrylic top. The sine sweeps were recorded using a dynamic analyzer, then postprocessing calculations converted the measured velocity to deflection at each frequency. A chamber pressure of 1 bar indicated that the chamber was vented to normal atmospheric conditions. A chamber pressure of 0 bar was the maximum vacuum obtained with an actual pressure of 0.06 bar, which was assumed to be representative of a perfect vacuum in this context. Natural frequency and damping results obtained from the frequency responses recorded indicated that the effects due to the presence of air caused the natural frequency to drop due to additional mass loading and increased the damping due to orifice losses. These effects were also observed to grow with driving frequency and voltage.

The parameters determined from the FE and CFD models were first tested in the FSI model in a state of negligible fluid effects implemented by setting the density and ambient pressure to one-thousandth of their normal ambient values. The results were compared with the frequency response of the deflection at 20, 40, and 60 V from the vacuum test, as illustrated in Fig. 6. The quasi-static response was observed at 200 Hz, where the deflection predicted by the FSI model at 40 V was 39 μm and compared with the experimentally determined value of 49 μm. The agreement was within 20% and was based strictly on calculations from the FSI model, with no empirical parameters except for the structural damping. Since the FSI model result was low, this indicated that the FE model was either predicting a piezoelectric force that was too low or an overall structural stiffness that was too high, resulting in a lower than expected deflection. Qualitatively, the FSI model predicted that the deflection increased with both frequency and voltage up to the peak deflection that occurred between 600 and 700 Hz, depending on the voltage. The peak deflection was lower than the natural frequency due to the relatively high structural damping. The drop in the peak frequency relative to the natural frequency was also a feature that was captured by the FSI model. Not captured was the experimentally observed tendency for the peak frequency to drop as a function of the amplitude of deflection. This may have been due to nonlinear stress softening effects at higher amplitudes. It must be noted that the frequency range of interest was between 200 and 500 Hz, below resonance. Although the discrepancy between the FSI model and the

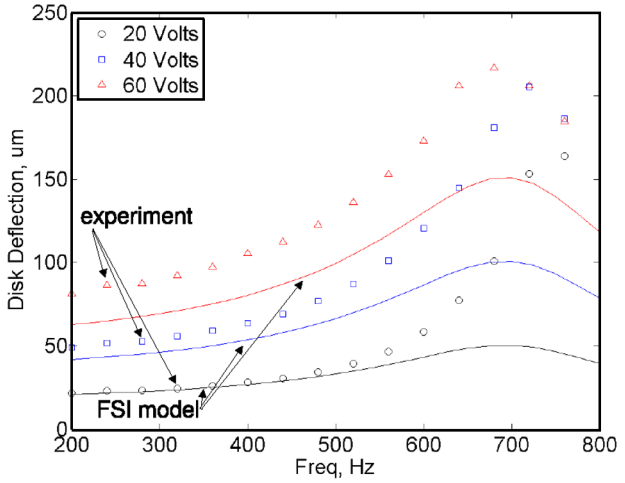

Fig. 6 Comparison of FSI model and experimental deflection in vacuum.

experimental results was pronounced at the peak response and higher frequencies, this was of less concern since it was outside of the frequency range of interest and illustrated in the figures for comparative purposes only. Since this stage of the validation relates to operation in a vacuum, there was no comparison to be made with the pressure and exit velocity. Next, the fluid (air) effects were included in the FSI model by setting the ambient pressure and density to their normal values of $P_0 = 110$ kPa and $\rho = 1.29$ kg/m^3. The frequency response of the deflection at 20, 40, and 60 V was plotted and compared with experimentally determined values at 1 atm of ambient pressure (roughly 1 bar), as shown in Fig. 7. Again, the main region of interest is between 200 and 500 Hz. The FSI model clearly captures the qualitative nature of the deflection frequency response, increasing with both frequency and voltage. The peak deflection is smaller in magnitude compared with the vacuum case and has shifted to lower frequency due to the mass loading effect of the air on the flexible structure and the damping. The relative experimental error for the deflection measurements is estimated at 8%. Although the laser vibrometer itself is much more accurate, uncertainty is introduced in the experimental procedure related to the location and angle of the laser target on the synthetic jet. Although there is some deviation in the qualitative values, the FSI model captures these important characteristics of the deflection frequency response.

B. Pressure Validation

The motion of the piezoelectric disks creates a pressure buildup in the cavity between the plates that, in turn, forces air out of the orifice. This internal pressure is a critical state variable directly related to synthetic jet operation and performance. Tests were conducted to characterize the internal pressure at various operating conditions. A test rig was designed and fabricated such that a single piezoelectric disk was mounted on a rigid top fixture disk with a hole in the center, as illustrated in Fig. 8. The top fixture disk mated with a bottom fixture disk that had a pressure sensor mounted at the center. The pressure sensor mounted on the bottom fixture disk protruded through the hole of the top fixture disk just below the piezoelectric disk when they were mated. A cavity beneath the piezoelectric disk was formed with a 1-mm-wide wall that was half of the typical height for a full synthetic jet. Including the 8 mm orifice, this formed an exact half-synthetic jet.

The pressure predicted by the FSI model in the frequency range of interest from 200 to 500 Hz is compared with experimental data, as illustrated in Fig. 9. The experimental data were obtained from the pressure tests described earlier using the half synthetic jets on a plate with a pressure transducer in the chamber. The relative experimental error was estimated at less than 3% based on preliminary calibration tests. The FSI model tends to underpredict the pressure. This is likely due to the underprediction of the deflection in the same frequency range. The qualitative nature of the pressure frequency response is

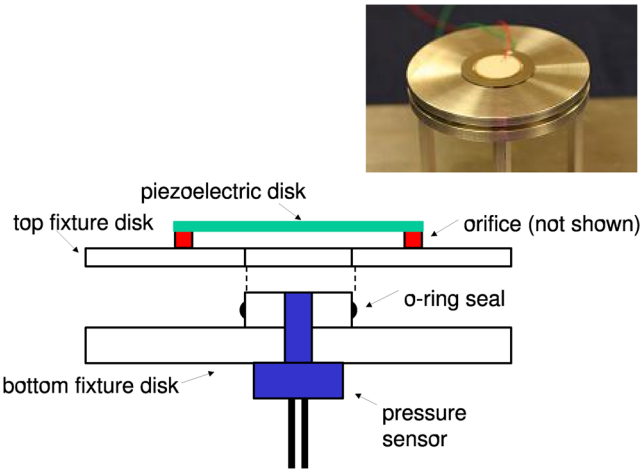

Fig. 8 The pressure test setup was half a synthetic jet with a pressure transducer underneath.

captured with the model, however, including the increase in pressure with frequency and voltage up to the peak pressure. At higher frequency past the peak pressure, the FSI model then tends to overpredict the pressure, also consistent with the trend in the deflection.

C. Exit Velocity Validation

The exit velocity of the air through the orifice is a critical parameter related to the cooling performance. Tests were conducted to measure and characterize the exit velocity. The tests were challenging due to the small scale of the flow. A hot-wire anemometer system was used to measure the exit velocity, as shown in Fig. 10. The hot-wire probe was positioned in front of the orifice to measure the exit velocity at a variety of positions, driving frequencies and voltages. The position of the hot wire was set according to its distance from the edge of the orifice. The active length of the hot wire was approximately the same as the height of the orifice, 1 mm, with a wire diameter of 50 μm. Therefore, it captured an average of the velocity profile across the height due to its vertical orientation. The hot wire was swept across the width of the orifice. At each position x, the synthetic jet driving frequency and voltage were swept from 100 to 800 Hz and 20 to 60 V, respectively. The transient exit velocity was recorded with a record length sufficient to resolve several ingestion/expulsion cycles at each position/frequency/voltage combination. The peak velocity from each transient wave form was then determined for use with further analysis. Note that the hot wire was swept in a plane along a straight line rather than along an arc tangent to the synthetic jet curvature. The

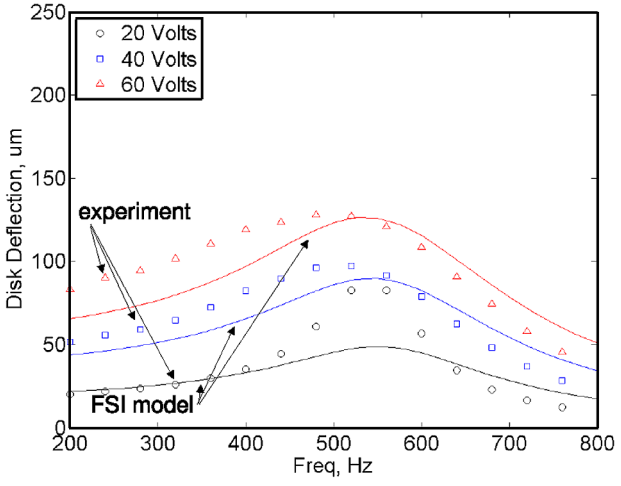

Fig. 7 Comparison of FSI model and experimental deflection at 1 bar ambient pressure.

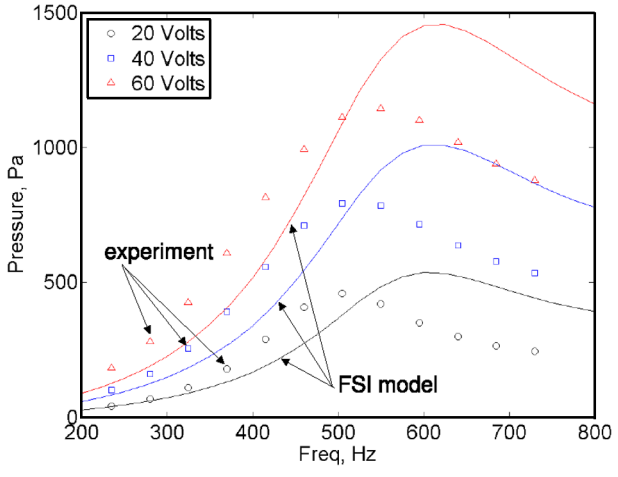

Fig. 9 Comparison of FSI model and experimental pressure.

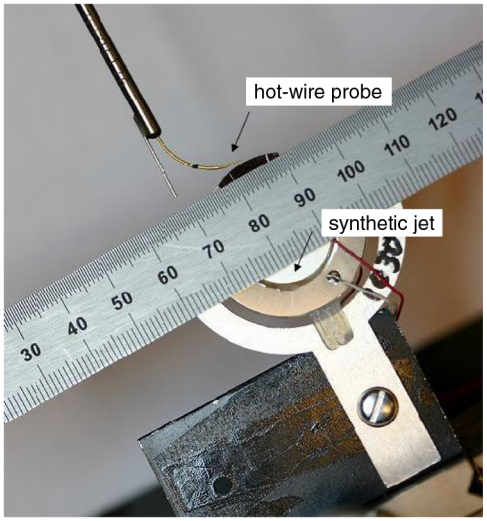

Fig. 10 Exit velocity test setup using hot-wire probe.

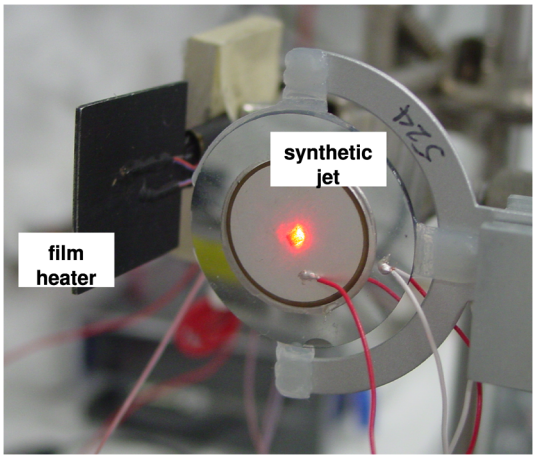

Fig. 12 The experimentally determined cooling performance of a synthetic jet is measured using an electric film heater and thermocouples.

closest measurement distance was approximately 1 mm at the center of the orifice.

The exit velocity predicted by the FSI model in the frequency range of interest is compared with the experimental data, as shown in Fig. 11. The experimental data were obtained from the hot-wire velocity measurements described earlier. The relative experimental error was estimated at 12% due to uncertainty in the hot-wire position and disturbance of the air flow around the sensor. The velocity was found to be mostly uniform across the orifice, except at resonance, so the average velocity amplitude is used for comparison in Fig. 11, and the assumption of uniform velocity distribution in the frequency range of interest was found to be reasonable. The FSI exit velocity is in good agreement with the experimental data up to 500 Hz, and the correct trends with frequency and voltage, observed in the other results, are also observed here.

D. Heat Transfer Validation

The most important function the synthetic jet provides is active cooling on a localized area. The cooling capability is determined by positioning the synthetic jet to cool an electric resistive heater over a range of driving voltages and frequencies, as shown in Fig. 12. An experimental rig named Rudy, in honor of Rudolf Clausius (one of the founders of modern day thermodynamics) was designed and built to facilitate characterization of synthetic jets. An input sequence is defined for each voltage, driving frequency, heater distance, and heater temperature of interest. A function generator creates a voltage sine wave that drives the synthetic jet, the heater distance is set by a three-axis stage, and the heater temperature is maintained at the desired level using a PID control. The steady-state DC heater voltage v_H and current i_H are recorded to determine the heater power p_H at each record of the input sequence as

$$p_H = v_H i_H \tag{30}$$

The value of EF is then calculated from Eq. (27), assuming the heater power is equivalent to the heat flux Q. EF tends to increase with voltage as expected. It is also highly dependent on the dynamic response of the synthetic jet structure. All of the data are stored in a relational database for subsequent postprocessing calculations and presentation.

The cooling effectiveness, or EF, predicted by the FSI model in the frequency range of interest up to 500 Hz is compared with the experimental data, as illustrated in Fig. 13. The experimental data were obtained from the heat transfer tests described earlier. The relative experimental error in the EF was expected to be 13% due to uncertainty in the temperature measurements, unknown conductive losses, and variable ambient conditions. Recall that the heat transfer correlation used in the FSI model [Eq. (28)] is specific to the film heater and geometry of the experimental setup. Nevertheless, it provides a useful indication and relative comparison to the cooling performance of synthetic jets. The FSI model predicts qualitative trends in the cooling performance that are consistent with the experimental data in the frequency range of interest. It tends to overpredict EF at higher frequency and voltage beyond resonance.

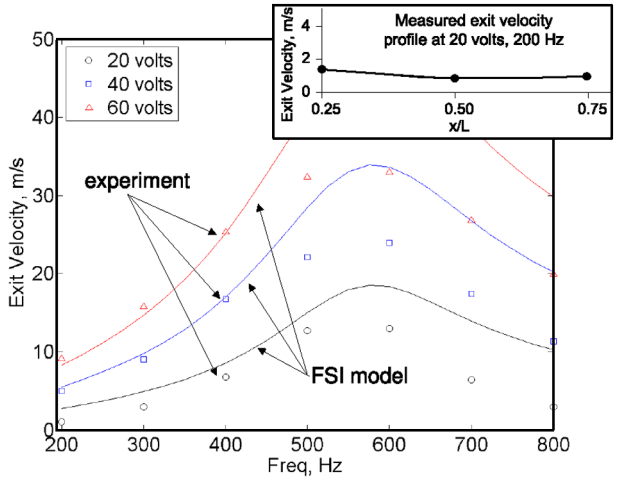

Fig. 11 Comparison of FSI model and experimental velocity averaged across the width of the orifice.

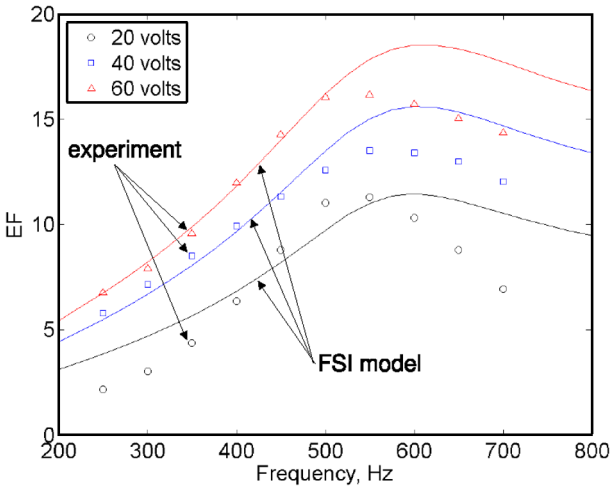

Fig. 13 Comparison of FSI model and experimental cooling performance EF.

The FSI EF predictive capability is still quite useful to uncover design trends and perform comparisons among candidate synthetic jets.

IV. Conlcusions

A practical FSI model to calculate synthetic jet performance and heat transfer enhancement was developed. The model is based on parameters obtained from running common FE and CFD models and accounts for the coupling between the piezoelectric actuators, structure, fluid, and heat transfer domains. Tests were performed to determine the behavior of the synthetic jet. Test results were compared with the FSI model results for validation, and the agreement was found to be good in the frequency range of interest.

Acknowledgments

This work was partially supported by the U.S. Department of Energy through contract DE-FC26-08NT01579. Special thanks to Charles Wolfe, Bryan Whalen, and Sitki Ulcay for their technical assistance. This report was prepared as an account of work sponsored by an agency of the U.S. Government. Neither the U.S. Government nor any agency thereof, nor any of their employees, makes any warranty, express or implied, or assumes any legal liability or responsibility for the accuracy, completeness, or usefulness of any information, apparatus, product, or process disclosed or represents that its use would not infringe privately owned rights. Reference herein to any specific commercial product, process, or service by trade name, trademark, manufacturer, or otherwise does not necessarily constitute or imply its endorsement, recommendation, or favoring by the U.S. Government or any agency thereof. The views and opinions of authors expressed herein do not necessarily state or reflect those of the U.S. Government or any agency thereof.

References

[1] Mittal, R., and Rampunggoon, R., "On Virtual Aero-Shaping Effect of Synthetic Jets," *Physics of Fluids*, Vol. 14, No. 4, 2002, pp. 1533–1536. doi:10.1063/1.1453470

[2] Lee, C. Y., and Glodstein, D. B., "DNS of Microjets for Turbulent Boundary Layer Control," AIAA 39th Aerospace Sciences Meeting and Exhibit, Reno, NV, AIAA Paper 2001-1013, 2001.

[3] Garg, J., Arik, M., Weaver, S., and Wetzel, T., "Meso Scale Pulsating Jets for Electronics Cooling," *Transactions of the ASME. Journal of Electronic Packaging*, Vol. 127, No. 4, 2005, Paper 503. doi:10.1115/1.2065727

[4] Mahalingam, R., and Glezer, A., "Design and Thermal Characteristics of a Synthetic Jet Ejector Heat Sink," *Journal of Electronic Packaging*, Vol. 127, No. 2, 2005, pp. 172–177. doi:10.1115/1.1869509

[5] Glezer, A., and Amitay, M., "Synthetic Jets," *Annual Review of Fluid Mechanics*, Vol. 34, Jan. 2002, pp. 503–529. doi:10.1146/annurev.fluid.34.090501.094913

[6] Erbas, N., Koklu, M., and Baysal, O., "Synthetic Jets for Thermal Management of Microelectronic Chips," International Mechanical Engineering Congress and Exposition 2005, American Soc. of Mechanical Engineers Paper 2005-81419, Fairfield, NJ, 2005.

[7] Arik, M., "Local Heat Transfer Coefficients of a High Frequency Synthetic Jets During Impingement Cooling over Flat Surfaces," *Heat transfer engineering*, Vol. 29, No. 9, 2008, pp. 763–773. doi:10.1080/01457630802053769

[8] Smith, D., Amitay, M., Kibens, V., Pareky, D., and Glezer, A., "Modification of Lifting Body Aerodynamics Using Synthetic Jet Actuators," 36th AIAA Aerospace Sciences Meeting and Exhibit, Reno, NV, AIAA Paper 1998-0209, 12–15 Jan. 1998.

[9] Crook, A., Sadri, A. M., and Wood, N. J., "The Development and Implementation of Synthetic Jets for the Control of Separated Flow," AIAA 17th Applied Aerodynamics Conference, Reno, NV, AIAA Paper 1999-3176, 1999.

[10] Mittal, R., Rampunggoon, P., and Udaykumar, H. S., "Interaction of a Synthetic Jet with a Flat Plate Boundary Layer," AIAA 31st Fluid Dynamics Conference and Exhibit, Norfolk, VA, AIAA Paper 2001-2773, 11–14 June 2001.

[11] Rathnasingham, R., and Breur, K. S., "System Identification and Control of Turbulent Boundary Layer," *Physics of Fluids*, Vol. 9, No. 7, 1997, pp. 1867–1869. doi:10.1063/1.869337

[12] Holman, R., Utturkar, Y., Mittal, R., Smith, B., and Cattafesta, L., "Formation Criterion of Synthetic Jets," *AIAA Journal*, Vol. 43, No. 10, 2005, pp. 2110–2116. doi:10.2514/1.12033

[13] Raju, R., Mittal, R., Gallas, Q., and Cattafesta, L., "Scaling of Vorticity Flux and Entrance Length Effects in Zero-Net-Mass-Flux Devices," AIAA 35th Fluid Dynamics Conference and Exhibit, Toronto, Ontario, AIAA Paper 2005-4751, 6–9 June 2005.

[14] Seeley, C. E., Arik, M., Hedeen, R., Uttukar, Y., Wetzel, T., and Shih, M. Y., "Coupled Acoustic and Heat Transfer Modeling of a Synthetic Jet," AIAA/ASME/ASCE/AHS/ASC 47th Structures, Structural Dynamics and Materials Conference, Newport, RI, AIAA Paper 2006-1879, 1–4 May 2006.

[15] Seeley, C. E., Arik, M., and Uttukar, Y., "Coupled Structural and Fluid Dynamics Modeling of a Synthetic Jet," 49th AIAA/ASME/ASCE/AHS/ASC Structures, Structural Dynamics, and Materials Conference, Schaumburg, IL, AIAA Paper 2008-1880, April 2008.

[16] Gallas, Q., Holman, R., Nishida, T., Carroll, B., Sheplak, M., and Cattafesta, L., "Lumped Elements Modeling of Piezoelectric-Drive Synthetic Jet Actuators," *AIAA Journal*, Vol. 41, No. 2, 2003, pp. 240–247. doi:10.2514/2.1936

[17] Clingman, D., "Development of an Aerodynamic Synthetic Jet Actuator Based on a Piezoelectric Buckled Beam," M.S. Thesis, Univ. of Maryland, College Park, MD, 2006.

[18] Sharma, R. N., "Fluid Dynamics Based Analytical Model for Synthetic Jet Actuation," *AIAA Journal*, Vol. 45, No. 8, Aug. 2007, pp. 1841–1847. doi:10.2514/1.25427

[19] William T. Thomson, *Theory of Vibration with Applications*, Prentice–Hall, Upper Saddle River, NJ, 1988.

[20] "ANSYS 8.0 User's Guide," ANSYS, Inc., Canonsburg, PA, 2003.

[21] Anderson, J. D., *Computational Fluid Dynamics*, McGraw–Hill, New York, 1995.

[22] "Icepak 4.4.8 Users' Manual," ANSYS, Inc., Canonsburg, PA, 2009.

[23] Holman, J. P., *Heat Transfer*, McGraw–Hill, New York, 2002.

[24] Boyce, W., and DiPrima, R., *Elementary Differential Equations*, 8th ed., Wiley, New York, 2008.

[25] "MATLAB R2008 User's Guide," Mathworks, Natick, MA, 2008.

[26] Arik, M., "An Investigation Into Feasibility of Impingement Heat Transfer and Acoustic Abatement of Meso Scale Synthetic Jets," *Applied Thermal Engineering*, Vol. 27, Nos 8–9, June 2007, pp. 1483–1494. doi:10.1016/j.applthermaleng.2006.09.027

B. Epureanu
Associate Editor